Journal of Applied Electrochemistry **34**: 671–680, 2004.

Segmented thin-gap flow cells for process intensification in electrosynthesis

S. RODE*, S. ALTMEYER and M. MATLOSZ
Laboratoire des Sciences du Génie Chimique, CNRS-INPL, Groupe ENSIC-Nancy, BP-451, 1 rue Grandville, F–54001 Nancy, France
*(*author for correspondence, e-mail: rode@ensic.inpl-nancy.fr)*

Received 20 May 2003; accepted in revised form 13 January 2004

Key words: current distribution, electrosynthesis, local process control, microreaction technology

Abstract

Design calculations are presented for a single-pass high-conversion electrochemical reactor suitable for process intensification in electroorganic synthesis. The key feature of the design is the use of a segmented working electrode, combined with a small anode–cathode gap. Each working electrode segment is operated at an optimal local current density, defined with respect to the local diffusion–limited current density of the reacting species. Two reactor configurations are considered: (i) an adiabatic reactor, and (ii) an isothermal reactor with integrated heat exchange. Calculated results for the devices in a classical electroorganic synthesis system, the methoxylation of 4-methoxytoluene, are presented and the general features and performance characteristics of the cell are compared with those of a more conventional capillary-gap cell, currently used industrially. For an electrode gap of 0.1 mm, the average current density attainable in the novel design is of the order of 2700 A m^{-2} in the adiabatic reactor and of the order of 7100 A m^{-2} in the isothermal reactor, respectively, 5 and 14 times higher than the current densities applied in the current industrial process. In addition to process intensification, other advantages of the proposed technology are the absence of reactant recycle, short residence times and plug flow of the reagents, all of which contribute to improved process selectivity.

List of symbols

C_A	reagent concentration (mol m^{-3})
c_p	specific heat capacity of the electrolyte (J kg^{-1} K^{-1})
d	interelectrode spacing (m)
D	diffusion coefficient of the reacting species (m^2 s^{-1})
f	ratio between the limiting and the applied current density
F	faradaic constant (96 487 C mol^{-1})
i	current density (A m^{-2})
i_{avg}	average current density (A m^{-2})
i_{lim}	limiting current density (A m^{-2})
I_{gl}	total applied current (A)
k_m	mass-transfer coefficient (m s^{-1})
L	total reactor length (m)
n	number of electrode sections in an individual cell
N	number of electrochemical cells in a reactor stack
n_e	number of electrons transferred in the reaction per mole of reagent
P_{des}	desired production rate (mol s^{-1})
ΔP	electrolyte pressure drop (Pa)
Q_{rev}	reversible heat generated by a cell reaction (J mol^{-1})
T	electrolyte temperature (K)
ΔT	local temperature increase (K)
ΔT_{gl}	global temperature increase (K)
u	fluid velocity (m s^{-1})
w	reactor width (m)

Greek symbols

η	irreversible overpotential of the electrodes (V)
Φ_{rev}	reversible cell potential (V)
$\Delta\Phi$	ohmic drop (V)
κ	electrolyte conductivity (Ω^{-1} m^{-1})
μ	liquid viscosity (kg s^{-1} m^{-1})
ρ	electrolyte density (kg m^{-3})
θ	local reagent conversion
θ_{gl}	global reagent conversion

Superscripts and subscripts

(k)	index of the electrode section
p	at constant pressure

1. Microstructured electrochemical reactor designs

The development of low-cost microfabrication technologies makes it possible to produce microstructured devices at competitive prices. Already routinely em-

ployed in laboratory apparatus and analytical equipment, the potential use of microstructured systems and components for chemical production has recently begun to be envisioned as well and has led to substantial rethinking of the way chemical reactors can be designed, built and operated. Indeed, new reactor concepts can now be proposed both to improve the performance of existing processes and to explore new or unusual reaction pathways that often appeared impossible or unrealistic for industrial development with existing technologies and classical designs [1, 2].

Microstructured systems are particularly promising in electrochemical reactor design. An overview of recent electrochemical process equipment used in industry, including divided and undivided cells, can be found in Lund and Hammerich [3]. The importance of the minimization of the anode–cathode gap was recognized early and has led to the design of capillary-gap cells with inter-electrode gaps on the millimeter scale [4]. Some other innovative microstructured electrochemical reactor designs are discussed below.

1.1. *Interdigitated band electrodes*

Belmont and Girault [5, 6] proposed a new type of electrosynthesis cell consisting of coplanar platinum interdigitated microband electrodes as shown in Figure 1(a). The fluid flows over the anode–cathode plate. The electrode width is in the range 0.5–1 mm, with a gap between the electrodes varying from 0.25 to 1 mm. This geometry results in anode/cathode distances of a few hundred micrometres thus minimizing ohmic penalties without hindering the hydrodynamics. At the same time, due to the periodic relaxation of the mass-transfer boundary layer, a significant enhancement of the mass-transfer coefficient to the electrodes is obtained. The experimentally determined mass-transfer coefficient is in the range $(3\text{–}7) \times 10^{-5}$ m s^{-1} and remains significant even in the absence of flow [6]. The authors conclude that this electrode geometry, restricted to undivided cells, could have interesting applications in tank reactors characterized by low convection regimes. The interest and the feasibility of the interdigitated electrode design has been demonstrated for furan methoxylation [6].

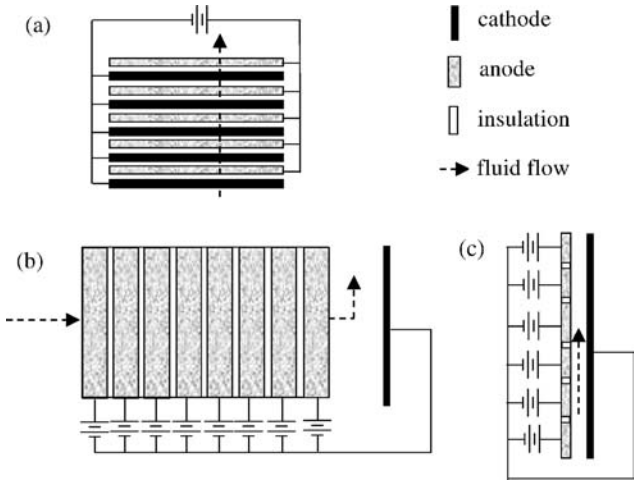

Fig. 1. Innovative electrode configurations. (a) Interdigitated microband electrodes, (b) multisectioned flow-through porous electrode and (c) segmented thin-gap electrode.

1.2. *Microchannel reactors*

Ziogas et al. [7] constructed with etching and laser techniques a miniaturized parallel plate electrochemical reactor containing 27 parallel channels. The anode material was glassy carbon and the cathode material stainless steel. The width of an individual channel was 800 μm, its length 64 mm and its height, corresponding to the cathode–anode distance, 25 μm. The reactor was cooled using an integrated heat exchanger. The test reaction was the methoxylation of 4-methoxytoluene, a reaction which will be discussed in more detail in Section 3. The solvent and co-reactant of the reaction is methanol. The initial concentration of 4-methoxytoluene was 2 mol l^{-1} (30% mass), with 0.01 mol l^{-1} (0.07% mass) of KF added as supporting electrolyte. The reactor was operated with a fluid velocity of 2.3 mm s^{-1} and a current density of 790 A m^{-2}. The reaction temperature was varied between 10 and 60 °C. Under these conditions, the reagent conversion was higher than 95%, with a selectivity of 80% and a current efficiency of 60%. The relatively low current efficiency observed is most probably due to the high reagent conversion, in a reactor designed for uniform spatial current distribution. Indeed, near the reactor outlet, where the conversion is high, the reagent concentration is very low, and side reactions may be significant. This interpretation is confirmed by experiments, performed at lower current densities (and without supporting electrolyte) for which the overall conversion was much lower (only 20%) but the measured selectivity and current efficiency much higher (respectively, 90% and 98%).

1.3. *Multisectioned flow-through electrode designs*

Matlosz [8] proposed a multisectioned flow-through porous electrode design permitting accurate control of local current distributions independently of the ohmic drop. The multisectioned porous electrode consists of alternating microstructures of conducting and insulating porous slices. Each conducting slice is connected to an independent current generator as shown in Figure 1(b). Since the electrical current flows parallel to the electrolyte fluid flow, the anode–cathode distances can be significant, resulting in a high average ohmic drop and substantial energy consumption. Despite this ohmic penalty, the configuration is convenient for cases is which anolyte–catholyte separation is necessary. A laboratory-scale demonstration unit with 10 independent slices has been designed, built and tested by Vallières and Matlosz [9]. A model electrosynthesis system consisting of oxidation of sodium gluconate to D-arabinose in competition with the parallel reaction of

oxygen evolution was chosen for investigation, and it was shown that the current efficiency could be significantly improved with the multisectioned design.

Bechthold and Turcanau [10, 11] applied this concept successfully in the vat dyeing industry. A standard dyeing apparatus for yarn on X-cones was coupled to a multicathode flow-through electrolyser for the indirect reduction of dispersed oxidized vat dyes. The vat dye was reduced by an iron (II/III)-triethanolamine complex which was regenerated continuously in the electrochemical cell. The catholyte was an alkaline solution (0.312 M NaOH) containing small amounts of the iron-triethanolamine complex (0.01 M). It was separated from the anolyte (1 M NaOH) by a cation exchange membrane. Current densities in the range 5–10 A m^{-2} were investigated and current efficiencies of 90% were attained.

The multisectioned flow-through design has thus proven its interest. Nevertheless, in cases where high current densities are desired and where the electrolyte conductivity is low, which is typically the case in organic electrochemistry, the ohmic penalty involved can be very high, thereby limiting the economic competitiveness of the design.

1.4. *Segmented thin-gap designs*

In the present work, an alternative to the multisectioned flow-through design is proposed. The alternative design, a segmented thin-gap cell, is shown schematically in Figure 1(c). The segmented design conserves the advantages of local control of current density, while the thin anode–cathode gap minimizes the ohmic drop. In the thin-gap design, the current flows perpendicularly to the fluid (a 'flow-by' approach) and the ohmic drop is therefore proportional to the width of the flow cell, which can be very small and is independent of electrode length. As in the design of the flow-through cell [8, 9], the working electrode is segmented by alternating conducting and insulating sections, and the length of the insulating sections is very small compared to the electrode section length. Each electrode section is connected to an independent current generator, thereby permitting electrical current modulation in space and in time. Scale-up of the electrochemical reactor can be achieved by cell stacking. The segmented thin-gap design provides significant opportunities for process innovation in organic electrochemistry by changing the classical process scheme. In the present work, an example application is studied, and the impact of the new design on process performance is discussed.

2. A single-pass high-conversion reactor for organic electrosynthesis

2.1. *Traditional low conversion process schemes*

Considering overall process economics, the product prepared by electrolysis should be obtained with high reagent conversion and high purity. With traditional, non-segmented reactor technologies two process schemes for this purpose are possible. A first process scheme consists of an electrochemical cell with low conversion per pass operated in batch mode (Figure 2(a)). The concentration of the reagent decreases with time and the process is stopped when the desired conversion is reached. Although the current distribution is uniform spatially within the electrochemical reactor, the applied current density must be lowered as a function of time, in order to adjust to the decreasing reagent concentration in the cell and avoid undesired side reactions. A disadvantage of this scheme is the batch mode of operation, which is poorly suited to high production rates.

A second well-known process scheme is an electrochemical cell with low conversion per pass operated in a continuous mode and placed in a recycle loop (Figure 2(b)). As in the previous scheme, the current distribution is uniform in space within the reactor. In order to work at high current density (high productivity), the reagent concentration in the loop should be as high as possible. The loop is continuously fed with fresh reagent and a fraction of the electrolyte is continuously withdrawn. The reagent and the product are then separated to concentrate the product and to recycle the reagent. The major disadvantage of this scheme is the complexity of the recycle loop and the large size of the separation units.

2.2. *Intensified high conversion process scheme*

With the use of segmented thin-gap cells for the desired reaction, an alternative to these traditional approaches

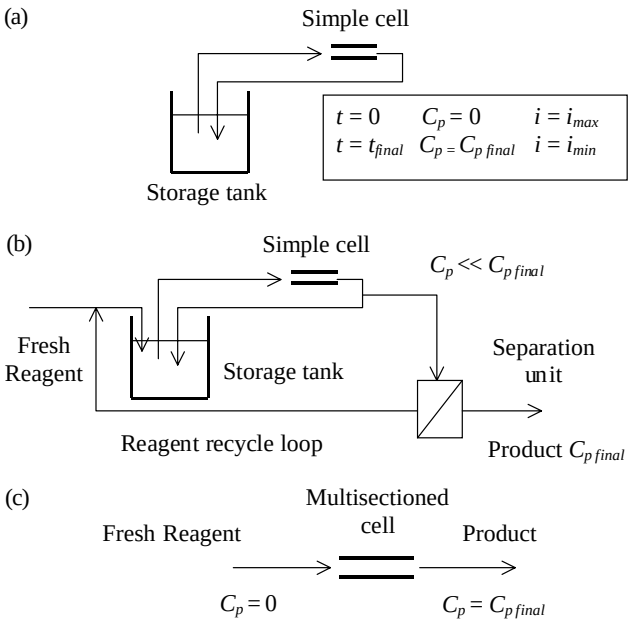

Fig. 2. Production schemes for organic electrosynthesis. (a) Batch, (b) continuous with reagent recycle and (c) single-pass high-conversion. C_p is the product concentration.

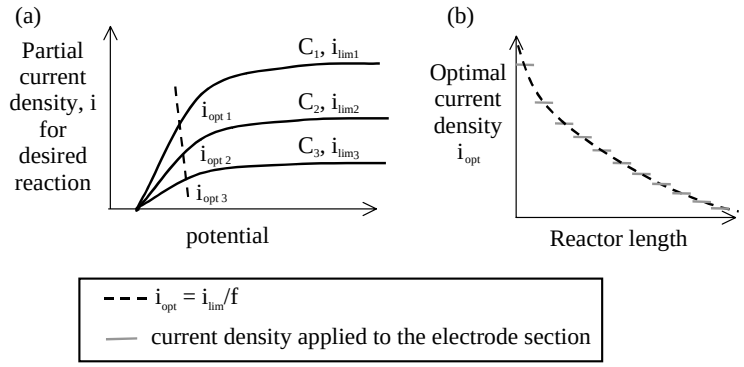

Fig. 3. Schematic presentation of the variation of the optimal current density in high conversion reactors. (a) Link between the limiting and the optimal current density and (b) variation of the optimal current density with the reactor length.

becomes possible: a single-pass high-conversion reactor (Figure 2(c)), a continuous process without recycle requiring only a small separation unit. Since the maximum local current density for the desired reaction, corresponding to the diffusion-limited current of the reagent, is proportional to the local reagent concentration, efficient use of the electrode surface without local side reaction can be attained by adjusting the local current density to a fraction (typically 50–70%) of the maximum diffusion-limited current density. If the conversion per pass is high, 50% or more, the reagent concentration and thus the limiting current density will vary strongly from the inlet to the outlet of the cell, as schematically shown in Figure 3(a). Electrode segmentation in such cases allows accurate adjustment of the local current density to the local reagent concentration, thereby permitting optimal use of the electrode as illustrated in Figure 3(b). Another important advantage of this alternative process scheme is the short residence time and the plug flow of the reagent, both of which minimize undesired consecutive reactions.

2.3. *Reactor model and design procedure*

To investigate the feasibility and the potential interest of a microstructured single–pass high–conversion electrochemical reactor, the optimal operating conditions must be defined and related to the major reactor characteristics: namely, overall conversion, θ_{gl}, overall temperature rise, ΔT_{gl} and average current density, i_{avg}.

The electrochemical reactor is composed of a stack of N electrochemical cells working in parallel. Each cell is comprised of two parallel plates, with interelectrode distance d, length L and width w, as shown in Figure 4. The working electrode of each cell is divided into n sections each of equal length, separated by thin insulating segments. In each electrode section, the local current density is adjusted in order to be optimal with regard to the local reagent concentration. Two reactor configurations are considered: (i) an adiabatic reactor, and (ii) an isothermal reactor with integrated heat exchange. A simplified approximate reactor model, suitable for preliminary investigation of the segmented thin-gap design has been developed for this case and is presented in Appendix A.

Different classes of parameters are necessary for the design of an individual electrochemical cell. A first class of parameters concerns the physico-chemical fluid characteristics and the reaction characteristics. The fluid parameters are the fluid density ρ, viscosity μ, electrical conductivity κ, and heat capacity c_p as well as the diffusion coefficient of the reagent species D. The reaction parameters are the reversible heat generated by the cell reaction Q_{rev}, the number of electrons exchanged n_e, and the overpotential η. The values of all these parameters are given by the electrochemical reaction system and the reaction temperature and cannot be freely chosen.

A second class of parameters concerns the geometrical cell characteristics and the operating parameters. The geometrical cell characteristics are the length of the cell L, its width w, the anode–cathode gap d and the number of sections n. The operating parameters are the ratio between the diffusion limited and the applied

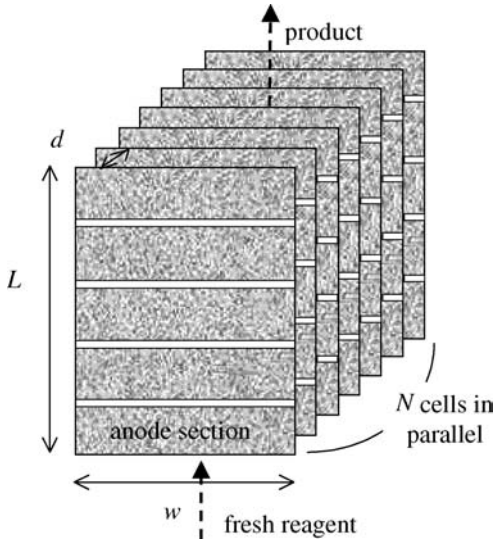

Fig. 4. View of a reactor stack with five electrode sections ($n = 5$).

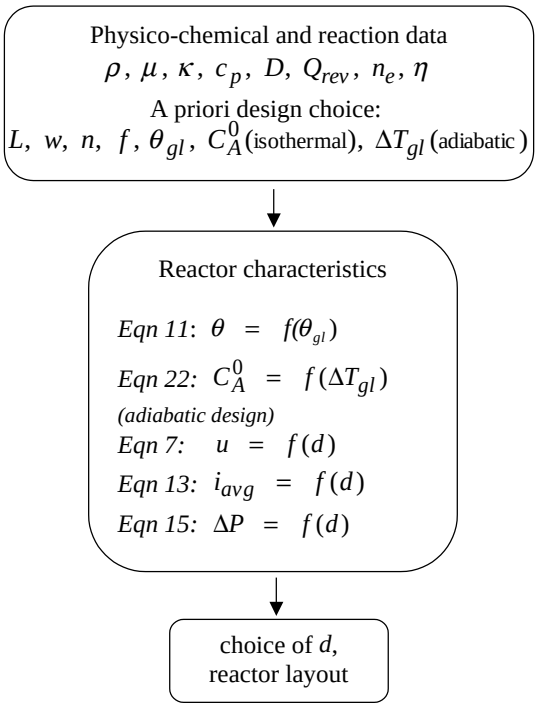

Fig. 5. Design procedure for an individual adiabatic electrochemical cell.

local current density f, the fluid velocity u and the input reagent concentration C_A^0. In contrast to the physico-chemical fluid characteristics and the reaction characteristics, the seven independent geometrical and operating parameters can be freely chosen in order to optimize the reactor design.

A possible design procedure is depicted in Figure 5. In the design procedure two of the independent design parameters, the fluid velocity u and the input reagent concentration C_A^0 are replaced for convenience by process constraints, namely the global reagent conversion θ_{gl} and the global temperature rise ΔT_{gl}. For the isothermal design, the global temperature rise is controlled by the integrated heat exchangers and the initial reagent concentration C_A^0 may be fixed freely. As illustrated in the following, the reactor performance is a strong function of the anode–cathode gap d.

3. Application: the anodic methoxylation of 4-methoxytoluene

3.1. *Reaction system*

The anodic methoxylation of 4-methoxytoluene leads to 4-methoxy-benzaldehyde-dimethylacetal which yields, after hydrolysis, anisaldehyde. The reaction route is shown in Figure 6. When methanol is used as a solvent, the reaction proceeds in a very fast two-electron oxidation of toluene to the benzylether followed by a subsequent fast two-electron oxidation of the benzylether to the diacetal [12, 13]. The counterelectrode reaction is hydrogen evolution.

The reaction is industrially performed by BASF with a production rate of 3500 tons per year [3]. The electrolysis step is performed in a capillary-gap cell and typical process parameters for that configuration are shown in Table 1. The cell is operated in a continuous mode and placed in a recycle loop, the production scheme is depicted in Figure 2(b). A process diagram including the separation steps is given in [3]. One of the major advantages of the process is that it can use methanol both as a solvent and as a reagent. Since methanol can be recycled conveniently, the process closes most loops, a decisive ecological advantage of this technology over 'classical' alternatives such as chlorination. The commercial benefits are also based on the high selectivity and the low energy demand of the total process. Both the acetal and the aldehyde can be used as intermediates for crop protection agents, fragrances, plating additives, ultraviolet absorbers, optical brighteners and other applications [3].

3.2. *Reactor layout*

To illustrate the reactor performance attainable with the segmented thin-gap cell, the design procedure shown in Figure 5 has been applied to the anodic methoxylation of 4-methoxytoluene. The estimated physicochemical data of the system as well as the design choices are given in Table 2. The overall conversion is fixed to a value of 0.9 for 10 independent electrode sections. For the adiabatic design, the reversible reaction heat Q_{rev} and the irrevers-

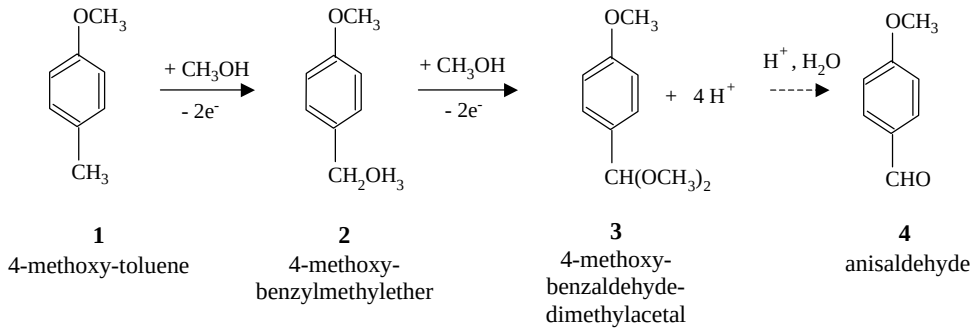

Fig. 6. Reaction scheme.

Table 1. Typical parameters for the BASF process for the anodic methoxylation of 4-methoxytoluene

Electrode material	Bipolar graphite rings
Interelectrode gap	0.5–1 mm
Substituted toluene	10–25% by mass (650–1650 mol m^{-3})
Supporting electrolyte	0.3–3% by mass potassium fluoride - sodium sulfonate
Methanol	90–75% by mass
Current density	300–500 A m^{-2}
Operating temperature	40–50 °C
Voltage per gap	4–6 V
Yield	>80%
Overall conversion	90–99%
Selectivity	85%

Table 2. Physico-chemical data for the system and design choices.

Physicochemical and reaction data at 40 °C	
Liquid density*, ρ/kg m^{-3}	850
Liquid viscosity*, μ/kg m^{-1} s^{-1}	0.00060
Specific heat capacity*, c_p/J kg^{-1} K^{-1}	2.38×10^3
Reagent diffusion coefficient**, D/m^2 s^{-1}	1.90×10^{-9}
Electrolyte conductivity***, κ/Ω^{-1} m^{-1}	2.0
Number of electrons involved, n_e	4
Reaction heat Q_{rev}/J mol^{-1}	neglected
Irreversible overpotential, η/V	neglected
A priori design choices	
Cell length, L/m	0.5
Cell width, w/m	0.5
Number of sections, n	10
Overall conversion, θ_{gl}	0.9
Resulting conversion per section θ (Equation 11)	0.206
Inlet reagent concentration, C_A^0/mol m^{-3} (isothermal design)	1650
Global temperature elevation, ΔT_{gl}/K (adiabatic design)	20
Resulting inlet reagent concentration, C_A^0/mol m^{-3} (Equation 22, adiabatic design)	620
Current factor f (as defined in Equation 3)	2
Desired overall production rate	
P_{des} (6000 h)/tons $year^{-1}$	3.500

* Weighed average of pure component properties for a reagent conversion of 50%. The physico-chemical characteristics of the reagent and the product are evaluated using its UNIFAC structure (evaluated using Pro II®)

** Determined using the procedure of Hayduk and Minas [14]

*** Estimated for 1.5% in mass KF electrolyte in methanol at 298° K

ible overpotential η are considered to be negligible in comparison to the Joule heating, and the temperature increase is limited to 20 K. The applied current density is adjusted locally to correspond to 50% of the limiting current density at the electrode section inlet ($f = 2$). The electrochemical reactor is calculated for an annual production rate of 3500 tons of anisaldehyde.

Figures 7, 8 and 9 present the variation of the major process parameters in a segmented cell for both the adiabatic and the isothermal reactor design and an inter-electrode gap varying from 0.01 to 1 mm. As shown in Figure 7, the fluid velocity, the mass-transfer coefficient and the pressure drop increase sharply with a decrease

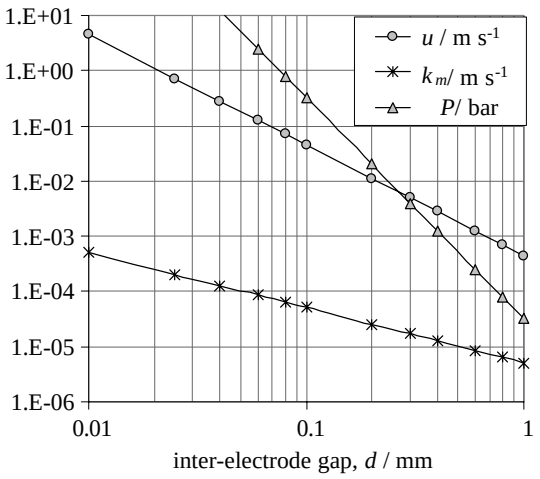

Fig. 7. Variation of major process parameters with the interelectrode gap for both the adiabatic and the isothermal design.

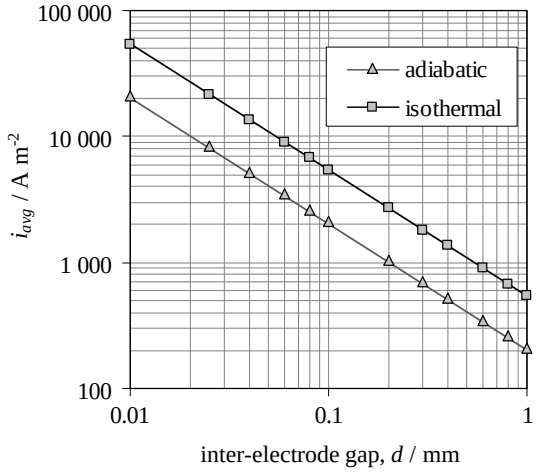

Fig. 8. Variation of the average current density with the interelectrode gap, comparison between the adiabatic and the isothermal design.

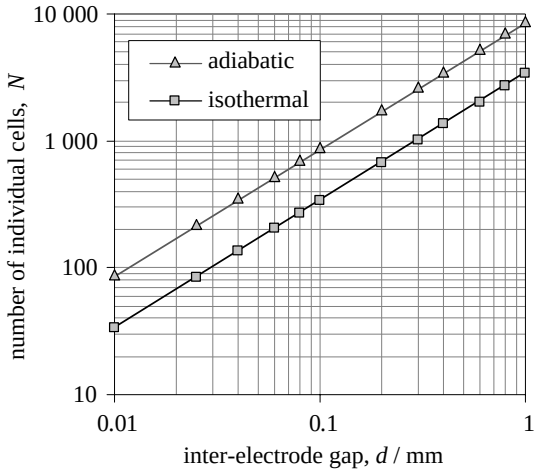

Fig. 9. Variation of the total number of electrochemical cells with the interelectrode gap, for an annual production of 3500 tons of anisaldehyde.

Table 3. Comparison of the performance of non segmented and segmented cells. Reactor and reaction characteristics as given in Table 2, isothermal design with an inter-electrode gap $d = 0.2$ mm. The current factor f is fixed to a value of 1.59 with respect to the outlet concentration of the electrode segment(s)

θ_{gl}(–)	Non-segmented cell, $n = 1$				Segmented cell, $n = 10$			
	u /m s^{-1} *Eqn 7*	ΔP /Pa *Eqn 15*	i_{avg} /A m^{-2} *Eqn 13*	N *Eqn 16*	u /m s^{-1} *Eqn 7*	ΔP /Pa *Eqn 15*	i_{avg} /A m^{-2} *Eqn 13*	N *Eqn 16*
0.2	1.61×10^{-1}	2.90×10^{4}	8206	224	1.78×10^{-1}	3.2×10^{4}	9091	202
0.4	6.04×10^{-2}	1.09×10^{4}	6154	299	7.68×10^{-2}	1.4×10^{4}	7828	235
0.6	2.68×10^{-2}	4.83×10^{3}	4103	448	4.20×10^{-2}	7.6×10^{3}	6413	287
0.8	1.01×10^{-2}	1.81×10^{3}	2051	897	2.31×10^{-2}	4.1×10^{3}	4699	392
0.9	4.47×10^{-3}	8.05×10^{2}	1026	1794	1.55×10^{-2}	2.8×10^{3}	3565	516
0.95	2.12×10^{-3}	3.81×10^{2}	513	3587	1.15×10^{-2}	2.1×10^{3}	2790	659

of the inter-electrode gap. These three parameters are identical for the adiabatic and the isothermal design. Figure 8 illustrates the variation of the average current density with the electrode gap in an adiabatic and in an isothermal cell. In the two cases, a decrease in the electrode gap results in a very significant increase in the average current density. The current densities attainable in the isothermal cell are naturally higher than those obtained in the adiabatic design, since under isothermal conditions much higher inlet reagent concentrations can be employed. Due to the higher average current densities, the number of electrochemical cells needed for a given annual production is lower in the isothermal design, compared to the adiabatic design, as illustrated in Figure 10. For the reactor length considered, attractive operating conditions are attained for an electrode gap of about 0.1 mm. Under these conditions, the fluid flow velocity is 6.2 cm s^{-1} and the pressure drop of the electrolyte is only 0.45 bar, very acceptable values.

Due to the limitation of the temperature rise in the adiabatic design, the acceptable initial reagent concentration is limited to 620 mol m^{-3}, which corresponds to 9.2% mass 4-methoxytoluene. This value is at the lower limit of the industrial production conditions (Table 1). For an electrode gap of 0.1 mm, the average current density is, nevertheless, about 2700 A m^{-2}, which is about five times higher than the performance of the current industrial process.

In the isothermal design with integrated heat-exchange, the inlet reagent concentration can be much higher. For an initial reagent concentration of 25% mass, an electrode gap of 0.1 mm leads to an average current density of 7100 A m^{-2}, which is more than 14 times higher than the current densities employed in the current industrial process. For the chosen cell geometry (50 cm long, 50 cm wide), only 258 segmented thin-gap cells in parallel are needed for the desired annual production.

As mentioned in Section 2.1, the high-conversion single-pass technology permits in addition a significant reduction in the dimensions of the downstream separation units. The design is also favourable to reaction selectivity, as the liquid is in plug flow and the resulting liquid residence time is quite short (8 seconds in the example calculations for an electrode spacing of 0.1 mm).

3.3. *Comparison with non-segmented designs*

High average current densities can be obtained in traditional capillary-gap designs at low conversion through reduction of the interelectrode gap. If a high reagent conversion par pass is desired, however, the segmented design permits much higher average current densities than those obtained in the traditional non-segmented design. In order to illustrate this statement, the reactor model established in Appendix A is applied to a segmented ($n = 10$) and a non-segmented ($n = 1$) design for global reagent conversions varying from 0.2 to 0.95. The calculations are performed for an isothermal reactor with an interelectrode gap of 0.2 mm and a current factor f of 1.59 with respect to the outlet concentration of each electrode segment.

Typical results are shown in Table 3. When the reagent conversion is increased, the liquid velocity, the pressure drop and the average current density decrease in the electrochemical cell, whereas the number of electrochemical cells needed for a given production increases. In the segmented design, however, the decrease of the average current density with increasing overall conversion is much less pronounced.

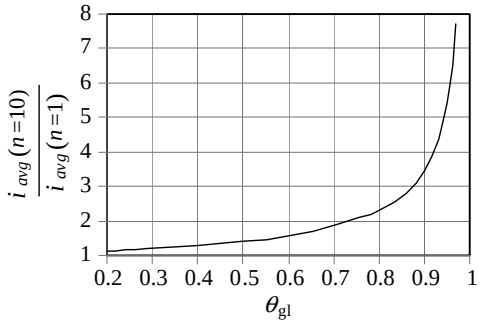

Fig. 10. Variation of the ratio between the current densities attainable in the segmented and the non-segmented design with the overall conversion. Conditions as for Table 4.

The decrease of the average current density with an increase of the reagent conversion is due to the fact that the most severe limit on acceptable current density occurs at the point of lowest reactant concentration (at the exit). For a non-segmented design, this limitation applies to the entire reactor whereas for a segmented design, only the segments near the exit are concerned. This difference in behavior is most pronounced for cases of high conversion, for which the reactant concentration at the exit is much lower, as illustrated in Figure 10 where the ratio of the current densities calculated by the reactor model using the segmented and the non-segmented design is plotted against the overall conversion. For desired overall conversion of 90%, the segmented design permits a more than three-fold increase in average current density for an identical interelectrode gap, in comparison to the traditional non-segmented capillary-gap design.

4. Conclusion

A simplified reactor model has been used to evaluate the potential interest of segmented thin-gap flow cells for process intensification in electrosynthesis. In particular, the possibility of employing segmented thin-gap cells effectively in single-pass high-conversion production schemes has been examined. Comparison of calculated performance at high conversion for the industrial methoxylation of 4-methoxytoluene illustrates the clear advantages of the segmented design in comparison to traditional non-segmented capillary-gap cells. Local control of the current density in the proposed segmented design permits use of significantly higher average current densities, thereby resulting in opportunities for highly intensified production. For the example examined in this study, for single pass conversion greater than 90%, the segmented thin-gap cell presents for identical electrode gap a more than three-fold increase in average current density in comparison to traditional thin-gap designs. The model calculations suggest that segmented thin-gap designs offer substantial opportunities for process intensification and radically improved process performance in organic electrosynthesis and encourage pursuit of experimental validation of the new technology for future industrial applications.

Acknowledgement

The authors wish to thank Degussa Corporation for financial support for major portions of this work.

References

1. W. Ehrfeld, V. Hessel and H. Löwe, 'Microreactors – New Technology for Modern Chemistry' (Wiley–VCH Verlag, Weinheim, 2000).
2. M. Matlosz and J.M. Commenge, *Chimia* **56** (2002) 654.
3. H. Lund and O. Hammerich, 'Organic Electrochemistry' (Marcel Dekker, New York , 4th (rev.) edn (2001).
4. R.E. Noftle and D. Pletcher, *J. Electroanal. Chem.* **227** (1987) 227.
5. C. Belmont and H.H. Girault, *J. Appl. Electrochem.* **24** (1994) 475.
6. C. Belmont and H.H. Girault, *J. Appl. Electrochem.* **24** (1994) 719.
7. A. Ziogas, H. Löwe, M. Küpper and W. Ehrfeld, *in* W. Ehrfeld (Ed), Third International Conference on 'Microreaction Technology', Proceedings of IMRET 3 (Springer, Berlin, 2000), p. 136.
8. M. Matlosz, *J. Electrochem. Soc.* **142** (1995) 1915.
9. C. Vallières and M. Matlosz, *J. Electrochem. Soc.* **146** (1999) 2933.
10. T. Bechthold, E. Burtscher, A. Turcanu and O. Bobleter, *J. Appl. Electrochem.* **27** (1996) 1021.
11. T. Bechthold and A. Turcanu, *J. Electrochem. Soc.* **149** (2002) D7.
12. H. Wendt and S. Bitterlich, *Electrochim. Acta* **37** (1992) 1951.
13. H. Wendt, S. Bitterlich, E. Lodowicks and Z. Liu, *Electrochim. Acta* **37** (1992) 1959.
14. 'Ullmann's Encyclopedia of Industrial Chemistry', Vol. B1 (VCH, Weinheim, 5th (rev.) edn 1990), p. 6.
15. D.J. Pickett, 'Electrochemical Reactor Design' (Elsevier Scientific, Oxford, 2nd edn 1979), Chapter 4.
16. J.S. Newman, 'Electrochemical Systems' (Prentice Hall, Englewood Cliffs, NJ, 2nd edn 1991), Chapter 13.

Appendix A: Reactor model

A.1. *Cell geometry*

The electrochemical reactor is composed of N electrochemical cells working in parallel. Each cell is comprised of two parallel plates with interelectrode distance d, length L and width w, as shown in Figure 4. The working electrode of each cell is divided into n sections with equal length, L/n, the conversion per section is small, that is, lower or equal to 0.2. The size of the insulating zone between sections is taken to be negligibly small and is not considered. In each section, the local current density is adjusted in order to be optimal with regard to the local reagent concentration. The principal features of an individual cell are shown in Figure 11.

A.2. *Estimation of the local mass transfer coefficient*

If the length of the insulating segments which separate the different electrode sections is small compared to the electrode section length, the relaxation of the mass-transfer boundary layer between two electrode sections can be neglected. In this case, the mass transfer boundary layer developed in the segmented electrochemical reactor is very similar to that developed in a parallel plate reactor with long electrodes.

In developed laminar flow with long electrodes, the mass transfer boundary layer spans the entire interelectrode gap. In this case, assuming a constant mass flux per unit area of electrode, a conservative estimation of the mass-transfer velocity, k_m, is given by [15]:

$$k_m = 2.692\frac{D}{d} \tag{1}$$

(The assumption of a constant surface concentration leads to $k_m = 2.43\ D/d$). The mass transfer velocity increases with the diffusion coefficient of the reagent, D, and with the decrease of the interelectrode spacing d but it does not depend on the fluid velocity.

A.3. *Maximal and optimal local current density*

The maximum current density which can be applied in section k, the diffusion limited current density designed by $i_{\lim}^{(k)}$, is a function of the mass transfer velocity, k_m, and the inlet reagent concentration of section k:

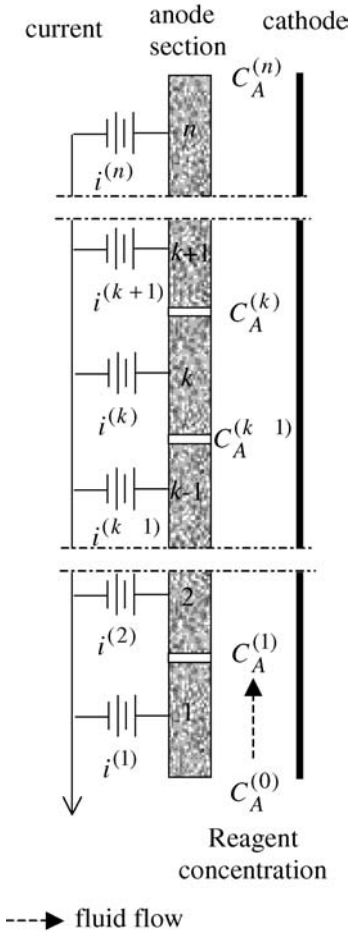

Fig. 11. Principal features of the electrochemical cell.

$$i_{\lim}^{(k)} = n_e F k_m C_A^{(k-1)} \tag{2}$$

The optimal operating current density can be defined with respect to the diffusion limited current density:

$$i^{(k)} = i_{\lim}^{(k)} \Big/ f = \left(\frac{2.692}{f}\right) n_e F C_A^{(k-1)} \left(\frac{D}{d}\right) \tag{3}$$

where f is typically comprised between 1.4 and 2. This current density is optimal because it is a significant fraction of the maximum diffusion-limited current density while at the same time minimizing side reactions. The optimal current density varies from one electrode section to another, since the reagent concentration decreases. If the length of the electrode section is large in comparison to the anode–cathode gap, the local current density distribution on each individual section can be considered to be uniform.

A.4. *Local and global conversion*

The conversion on electrode section k can be evaluated by a mass balance on the reagent passing through the section:

$$udwC_A^{(k-1)} = udwC_A^{(k)} + \left(\frac{i^{(k)}}{n_e F}\right)\left(\frac{Lw}{n}\right) \tag{4}$$

where u is the flow velocity of the electrolyte. The conversion is given by

$$\theta^{(k)} = \frac{C_A^{(k-1)} - C_A^{(k)}}{C_A^{(k-1)}} = \left(\frac{i^{(k)}}{n_e F}\right)\left(\frac{1}{udC_A^{(k-1)}}\right)\left(\frac{L}{n}\right) \tag{5}$$

Substituting the local current density by its expression given in Equation 3, the conversion can be expressed as a function of the geometric and operational parameters. Thus,

$$\theta^{(k)} = \theta = \left(\frac{2.692}{f}\right)\left(\frac{L}{n}\right)\left(\frac{D}{d^2 u}\right) \tag{6}$$

If all electrode sections have the same length, they yield the same local conversion θ. Equation 6 permits calculation of the fluid velocity for a given local conversion:

$$u = \left(\frac{2.692}{f}\right)\left(\frac{L}{n}\right)\left(\frac{D}{\theta d^2}\right) \tag{7}$$

The reagent concentration at the outlet of electrode section k is given by

$$C_A^{(k)} = C_A^{(k-1)}(1-\theta) \tag{8}$$

The outlet concentrations of the different sections can be combined to obtain a relation between the reactor inlet and outlet concentrations. Thus,

$$C_A^{(n)} = C_A^{(0)}(1-\theta)^n \tag{9}$$

The global conversion can thus be calculated, based on the conversion per section and the number of sections:

$$\theta_{gl} = \frac{C_A^{(0)} - C_A^{(n)}}{C_A^{(0)}} = 1 - (1-\theta)^n \tag{10}$$

Equation 10 may be used to determine the conversion per section, if the overall conversion and the number of sections are given. That is,

$$\theta = 1 - (1-\theta_{gl})^{1/n} \tag{11}$$

A.5. *Average current density, pressure drop and number of cells in parallel*

The average current density is the overall applied current divided by the electrode surface. Thus,

$$i_{avg} = \frac{I_{gl}}{wL} = \frac{n_e F u d C_A^{(0)} \theta_{gl}}{L} \tag{12}$$

When substituting the flow velocity using Equation 7:

$$i_{avg} = \left(\frac{2.692}{f}\right)\left(\frac{n_e F D C_A^{(0)}}{d}\right)\left(\frac{\theta_{gl}}{n\theta}\right) \tag{13}$$

The average current density increases with decreasing electrode spacing and reactors with small electrode spacing can operate at higher current densities than reactors with larger spacing.

The pressure drop for developed laminar flow between two flat plates is given by

$$\Delta P = \frac{24 \mu u L}{d^2} \tag{14}$$

when substituting the flow velocity:

$$\Delta P = \left(\frac{64.6}{f}\right)\left(\frac{D\mu}{n\theta}\right)\left(\frac{L^2}{d^4}\right) \tag{15}$$

The number of electrochemical cells operated in parallel, N, depends on the desired production rate P_{des}:

$$N = \frac{P_{\text{des}}}{udwC_A^{(0)}\theta_{\text{gl}}} = \left(\frac{P_{\text{des}}}{DC_A^{(0)}}\right)\left(\frac{f}{2.692}\right)\left(\frac{d}{wL}\right)\left(\frac{n\theta}{\theta_{\text{gl}}}\right) \tag{16}$$

The number of cells decreases with decreasing electrode spacing. This is due to the increase of the average current density in small gap cells.

A.6. *Local and global temperature rise in an adiabatic reactor design*

The adiabatic reactor design, which is the simplest to build, is only possible if the temperature rise of the reactive flow is restricted to a reasonably low value. The temperature rise is mainly due to the Joule heating of the solution induced by the current flow through the electrolyte. Secondary heat sources are the reversible heat due to the reaction itself Q_{rev}, and the heat generation due to the irreversible overpotential of the electrode surface η. The reaction heat is related to the entropy change for the overall cell reaction which can be obtained from the temperature coefficient of the reversible cell potential [16]. For section k, one obtains:

$$Q_{\text{rev}} = \frac{i^{(k)}wL}{n} T\left(\frac{\partial\Phi_{\text{rev}}}{\partial T}\right)_p \tag{17}$$

The temperature rise in section k can be evaluated by a local heat balance:

$$\rho c_p udwT^{(k-1)} + \frac{i^{(k)}wL}{n}\left(\Delta\Phi^{(k)} + \eta + T\left(\frac{\partial\Phi_{\text{rev}}}{\partial T}\right)_p\right) = \rho c_p udwT^{(k)} \tag{18}$$

with the local ohmic drop in a flat cell geometry given by

$$\Delta\Phi^{(k)} = \frac{i^{(k)}d}{\kappa} \tag{19}$$

The temperature rise in section k is thus given by

$$\Delta T^{(k)} = T^{(k)} - T^{(k-1)} = \frac{L}{n}\frac{i^{(k)}}{\rho c_p ud}\left(\frac{i^{(k)}d}{\kappa} + \eta + T\left(\frac{\partial\Phi_{\text{rev}}}{\partial T}\right)_p\right) \tag{20}$$

When substituting the local current density and the flow velocity using Equations 3 and 7, the temperature rise in section k can be expressed as a function of the inlet reagent concentration, the physico-chemical characteristics of the system and the local conversion. Thus,

$$\Delta T^{(k)} = \frac{n_e F C_A^{(k-1)}\theta}{\rho c_p}\left[\left(\frac{2.692}{f}\right)\left(\frac{n_e F C_A^{(k-1)} D}{\kappa}\right) + \eta + T\left(\frac{\partial\Phi_{\text{rev}}}{\partial T}\right)_p\right] \tag{21}$$

The global temperature rise of the solution is the sum of the temperature rise of each section. That is,

$$\Delta T_{\text{gl}} = \sum_{k=1}^{n}\Delta T^{(k)} = \frac{n_e F C_A^0\theta_{\text{gl}}}{\rho c_p}\left[\left(\frac{2.692}{f}\right)\left(\frac{n_e F C_A^0 D}{\kappa}\right) \times \left(\frac{2-\theta_{\text{gl}}}{2-\theta}\right)\eta + T\left(\frac{\partial\Phi_{\text{rev}}}{\partial T}\right)_p\right]$$

It can be seen that a limitation of the total temperature rise implies for a given reaction system and a given conversion, an upper limit on the input reagent concentration.